Thermodynamic of liquid metal infiltration in TiC-SiC or SiC porous compacts

Jérôme Roger, Marie Salles

Thermodynamic of liquid metal infiltration in TiC-SiC or SiC porous compacts

Jérôme. Roger [a,*], Marie. Salles[a]

[a] Université de Bordeaux, CNRS, Laboratoire des Composites ThermoStructuraux, UMR 5801, 33600 Pessac, France

* Corresponding author: e-mail: jerome.roger@lcts.u-bordeaux.fr

Abstract

This work is the study of the reactivity during the capillary infiltration of liquid silicon or Si-Ti molten alloys in SiC or SiC+TiC compacts to form $TiSi_2$/SiC composites. The main aim was to identify the thermodynamic and kinetic limitations of this process. Preliminary thermodynamic analyses of the equilibria in the Ti-Si-C system were performed to select the compositions of the liquid and the operating temperatures. Three cases were chosen: 1) infiltration of molten $TiSi_2$ in pure SiC compacts at 1550°C, 2) reactive infiltration of pure liquid silicon in SiC+TiC compacts at 1450°C, and 3) reactive infiltration of the molten eutectic $Ti_{0.16}Si_{0.84}$ alloy in SiC+TiC compacts at 1380°C. The compacts were prepared from mixtures of micronic SiC (α or β polytypes) and TiC powders. The compositions of the powder mixtures were calculated to fill totally the porosity of the compacts of about 50% or with an excess of TiC. The heat treatments of the pellets at 1380, 1450 and 1550°C were performed with a holding duration of 1 h in high vacuum. Experimental results evidenced that the interactions between the liquid and the powders are complex. The obtained materials differ more or less from the expected composites that are generally not dense and contain variable quantities of free silicon. It is found that these experimental results can be explained by advanced thermodynamic calculations. This work proves that the activity gradients play a determining role during the infiltration process by initiating the dissolution and the diffusion of atoms in the liquids.

Keywords: A Ceramics; A Composite materials; B Liquid-solid reactions; C Diffusion; C Phase diagrams; C Microstructure

1. Introduction

$TiSi_2$ is very attractive for high temperature applications. Indeed, this compound exhibits a congruent melting at high temperature (1500°C), a low density (4.08 $g.cm^{-3}$), a high modulus at room temperature (255.6 GPa) and excellent oxidation resistance [1,2]. The thermal and electrical conductivities are relatively high, making this compound attractive for electronic interconnection and diffusion barrier [3]. But this compound is very brittle and exhibits a low strength at high temperature. The solution considered by some authors to improve the thermo-mechanical properties of this intermetallic phase is the addition of a second phase to produce composites [4-8]. On this way, SiC is an interesting reinforcement material for $TiSi_2$. Indeed, SiC is chemically compatible with $TiSi_2$ [9]. Furthermore, silicon carbide is an attractive ceramic, due to its properties: low bulk density, high toughness, wide band gap, high oxidation resistance, high thermal stability and conductivity [10-13]. The application range of this material is wide and include components for advanced propulsion systems, energy conversion devices, and other high-temperature structures. However, the elevated mismatch of the thermal coefficients of these compounds (9.0×10^{-6} K^{-1} for $TiSi_2$, 4.8×10^{-6} K^{-1} for SiC) could generate deleterious cracks depending on the size of the SiC grains [14]. SiC/$TiSi_2$ composites were successfully prepared by some authors first by hot pressing mixed powders of TiC, Ti and Si at 1380°C to avoid the melting the silicon ($T_{melting}$(Si)=1410°C) [14,15]. The obtained materials contained up to 34 vol% of SiC with a maximal density of 99%. Due to the elaboration method which induces a noticeable shrinkage, the size and shape of the material are limited. $TiSi_2$/SiC composites were also successfully synthesized by high-temperature-induced heat combustion synthesis with interesting densification and mechanical properties [16]. But, these two techniques are limited to small pieces. An alternative way to increase the SiC content and to produce large composites is liquid silicon infiltration (LSI) in SiC/TiC tapes. The recent work reported by M. Sun et al. shows that it is possible to synthesize this kind of composites from laminated SiC/TiC tapes with 0.2 mm thickness [15]. The reaction between TiC and liquid silicon at 1550°C for 1 h under vacuum leads successfully to the formation of SiC+$TiSi_2$

composites with a promising mechanical behavior. Despite these progresses, the synthesis of this kind of material by infiltration at elevated temperature still has limitations, especially because of the reactivity. The development of this process requires a better knowledge and a thorough understanding of the thermodynamic and kinetic processes involved. On this way, the aim of the present work consists in studying the elaboration of $TiSi_2$/SiC composites by capillary infiltration of liquid silicon or Si-Ti molten alloys in SiC of SiC+TiC compacts. Three cases are examined below: 1) infiltration of molten $TiSi_2$ in pure SiC compacts, 2) reactive infiltration of pure molten silicon in SiC+TiC compacts, 3) reactive infiltration of the eutectic $Ti_{0.16}Si_{0.84}$ alloy in SiC+TiC compacts. The corresponding working temperatures were taken a few degrees above the melting point, i.e. 1550°C for molten $TiSi_2$, 1450°C for liquid Si and 1380°C for the eutectic liquid. In this way, it is possible to identify the best way, the limiting phenomenon and their thermodynamic and kinetic origins.

2. Experimental

2.1 Thermodynamic assessments of the Ti-Si-C system

Prior to the experimental investigation, preliminary thermodynamic analyses of the equilibria in the Ti-Si-C system were performed with Thermo-Calc software [17]. The thermodynamic equilibria calculated from this software were based on the CALculation of PHAse Diagrams (CALPHAD) methodology [18,19]. The relevant thermodynamic description of this ternary system reported by Y. Du et al. was used for these calculations [20]. The calculated Ti-Si-C phase diagram at 25°C is shown in Figure 1-a) highlighting that $TiSi_2$ and SiC are in equilibrium at this temperature. In the Ti-Si phase diagram shown in Figure 1-b) are given the formation temperatures of liquid on the Si-rich side. Three liquids were considered in this study corresponding to pure Si ($T_{melting}$ = 1410°C), the eutectic alloys $Ti_{0.16}Si_{0.84}$ ($T_{melting}$ = 1330°C) and $TiSi_2$ ($T_{melting}$ = 1500°C). These compositions were chosen because of their different titanium content and various melting temperature.

2.2 Materials and experimental procedures

Commercial α-SiC and β-SiC powders (d_{50} = 2 µm, 99.8% purity, Alfa Aesar GmbH & Co KG, Germany); and a TiC powder (d_{50} = 2 µm, 99.5% purity, Alfa Aesar GmbH & Co KG, Germany) were used as raw material for the preparation of the compacts. $TiSi_2$ powder (d_{50} = 44 µm, 99.5% purity, Alfa Aesar GmbH & Co KG, Germany); silicon chips (1-3 mm, 99.9999%, Strem Chemicals, Inc., Germany); and silicon powder (d_{50} = 44 µm, 99.999% purity, Alfa Aesar GmbH & Co KG, Germany); were used as source materials for the liquids. The porous SiC and TiC-SiC compacts were obtained from pure SiC powders and from mixtures of the SiC and TiC powders, respectively. The mixed TiC and SiC powders were blended in a mixture of alcohol (50 vol%) and water (50 vol%). After drying, the powders were uniaxially cold pressing into rectangular specimens at 100 MPa using a stainless-steel die with an addition of 1 cm^3 of commercial ethanol. Then, after drying in the atmosphere for 12 h, the green compacts were presintered at 1500°C for 1 h under high vacuum (2.10^{-4} mbar) to obtain strengthened porous ceramics. The compositions of the mixtures were chosen to fill totally the porosity of the compacts, of about 50%, after reaction with the liquid or with an excess of TiC. Details characteristics of the six samples of this study are given in Table 1. The porosity was measured by helium pycnometry (Autopore IV, Micromeritics Instrument Corp., USA). The heat treatments of the pellets at 1380, 1450 and 1550°C were performed in an inductively heated graphite susceptor with heating and cooling rate of 20°C.min^{-1} and holding time of 1 h in high vacuum (2.10^{-4} mbar). The control of the temperature was done by pyrometry. As shown in Figure 2, the samples were inserted in alumina crucibles. Their inner faces were sprayed-coated by BN in the case of molten silicon as anti-wetting (HeBoCoat 21E, Henze Boron Nitride Products AG, Germany). The amount of liquid used in each experiment was taken with an excess of 10% in mass. After cooling, the samples were cross-cut in the length and polished drown to a 1 µm diamond finish. An overview of each sample was obtained from about 100 pictures taken with an optical Nikon ME600L microscope, the overall image was reconstructed with Image Analysis System (*ImageJ*) [21]. The microstructures of the samples were examined

with a FEI Quanta 400FEG scanning electron microscopy (SEM) operated at 10 kV. From backscattered-electrons (BSE) micrographs and Image Analysis System (*ImageJ*), it was possible to estimate the depth of the infiltration fronts, the phases present and their proportions in the different areas of the samples. To measure atomic composition profiles, the infiltration area of each compact was analyzed with an electron probe microanalyzer (EPMA, Cameca SX-100) with wavelength-dispersive spectrometers (WDS). The errors of carbon determinations via EDS and WDS techniques are estimated to ±5% and ±2%, respectively. Because of the smallness of the grains, a large scanning probe surface of 30×30 μm^2 with steps of 60 µm was used for WDS measurements.

3. Results

3.1 Thermodynamic calculations

The aim of this work is to examine the mechanisms occurring during the liquid infiltration into porous compacts to synthesize $TiSi_2$/SiC composites. The selection of the compositions of the liquids and their operating temperature was based on thermodynamic calculations. As mentioned herein, three compositions were identified from the Ti-Si phase diagram (Fig. 1-b)) corresponding to three different ways of synthesis, the corresponding thermodynamic calculations are detailed below. The first way involves the capillary infiltration of molten $TiSi_2$ into SiC compacts at a temperature higher than 1500°C. The choice was done to operate in each case at a temperature 30 or 50°C above the melting temperature to make sure of the total melting. The first case corresponds to the section of the Ti-Si-C phase diagram calculated at 1550°C and shown in Figure 3-a). This section reveals that SiC and molten $TiSi_2$ are not in equilibrium at this temperature and should react. The SiC-$TiSi_2$ isopleth calculated at 1550°C (Fig. 4-a)) shows that SiC and $TiSi_2$ are in equilibrium for temperatures lower than 1462°C. The calculation of the volume fractions of the phases for the SiC-$TiSi_2$ isopleth at 1550°C (Fig. 5-a)) confirms that the volume fraction of SiC is lower than the initial 50 vol% when

considering a compact exhibiting a porosity of 50%. The corresponding mole fraction of $TiSi_2$ is equal to 0.32, this value is marked by a dotted blue line in Figure 4-a), Figure 5-a) and Figure 6-a). This decrease of the SiC fraction is justified by the formation of the Ti_3SiC_2 compound but also by the dissolution of a small amount of SiC in the liquid to reach the atomic composition Ti:Si:C = 26.07:73.78:0.15 (Figure 6-a). At the cooling, the final composition of the composite is expected to be 51 vol% of SiC and 49 vol% of $TiSi_2$, as shown in Figure 5-b). A black five-pointed star indicates the composition of this $TiSi_2$-SiC ceramic in Figure 3-a). It can be expected that the infiltration mechanism of molten $TiSi_2$ follows the stages describes in Figure 7-a) with the infiltration of the liquid and its saturation by dissolution of a small amount of SiC. The precipitation of Ti_3SiC_2 cannot be excluded, especially when its driving force of formation is higher than the one of SiC (Figure 8-a)). During the cooling, when the temperature goes below 1462°C, the ternary liquid reacts with Ti_3SiC_2 grains to form SiC and $TiSi_2$. The second case uses the $Ti_{0.16}Si_{0.84}$ eutectic liquid which melts at a temperature of only 1330°C. This composition was considered as interesting because of its lower temperature of melting and its low titanium content. It is then necessary to add TiC in the compact to obtain a pure $TiSi_2$-SiC ceramic. In the case of an initial porosity of 50%, the mass and volume ratios between TiC and SiC were calculated equal to $\frac{m_{TiC}}{m_{SiC}} = 0.49$ and $\frac{V_{TiC}}{V_{SiC}} = 0.32$, respectively. This composition is identified by a **X** on the Ti-Si-C phases diagram calculated at 1380°C (Figure 3-b)). According to this phase diagram, the reaction between TiC and the liquid should lead to the formation of $TiSi_2$ and SiC according to Equation 1:

$$\boldsymbol{TiC_{(S)} + \frac{75}{13}\, Ti_{0.16}Si_{0.84\,(L)} \rightarrow \frac{25}{13}\, TiSi_{2(S)} + SiC_{(S)}} \qquad \text{Equation 1}$$

This reaction implies the formation of $TiSi_2$ and SiC with an increase in the solid volume of +413%. The final composition of the $TiSi_2$-SiC ceramic is marked by a blue five-pointed star in Figure 3-b). The isopleth calculated between the **X** and $Ti_{0.16}Si_{0.84}$ compositions (Figure 4-b)) shows that for temperatures higher than 1330°C, $TiSi_2$ and SiC are in equilibrium with the starting liquid only at 1330°C. For higher temperatures, the atomic composition of the liquid in

presence of $TiSi_2$ and SiC evolves towards Ti:Si:C = 19.551:80.435:0.014 (Figure 6-b). This implies that during the infiltration of the liquid, this last one may dissolve Ti and C atoms from TiC. In the same time, the reaction corresponding to Equation 1 should occur and the progression of this reaction can be considered according to Figure 5-c) which indicates that the final ceramic is composed of 52 vol% of SiC and 48 vol% of $TiSi_2$. According to Figure 8-b), SiC should be formed first as its driving force of formation is vastly superior to the one of $TiSi_2$. No other phase is expected to be formed in contact with the liquid. Consequently, an infiltration mechanism is proposed in Figure 7-b) with first the partial dissolution of TiC followed by the precipitation of $TiSi_2$ and SiC leading to the filling of the pores. One has to note that the progressive filling of the layers at the bottom of the compact may gradually limit the liquid flow. The third case consists of the reactive infiltration of molten pure Si in SiC-TiC compacts at a temperature of 40°C higher than the melting temperature of silicon. The corresponding section of the Ti-Si-C phases diagram at 1450°C is given in Figure 3-c). It shows clearly that molten pure Si reacts with TiC to generate $TiSi_2$ and SiC, according to Equation 2:

$$\boldsymbol{TiC_{(S)} + 3\,Si_{(L)} \rightarrow TiSi_{2(S)} + SiC_{(S)}} \qquad \text{Equation 2}$$

This reaction occurs with an increase in the solid volume of +216%. For an initial porosity of 50%, the required mass and volume ratios between TiC and SiC were found equal to $\frac{m_{TiC}}{m_{SiC}} = 1.32$ and $\frac{V_{TiC}}{V_{SiC}} = 0.86$, respectively. This composition is identified by a **Y** in the figures relative to this case. The isopleth between the **Y** composition and pure Si, shown in Figure 4-c), highlights that at 1450°C the liquid must react with TiC by precipitating $TiSi_2$ and SiC while filling the pores. This case differs from the previous one by the higher working temperature (+70°C) and the elevated solubility of titanium and carbon in the liquid. Indeed, the atomic composition of the liquid in equilibrium with $TiSi_2$ and SiC was calculated to be Ti:Si:C =25.08:74.87:0.05 (Figure 6-c). According to Figure 5-d), the final composition is expected to reach 51 vol% of SiC and 49 vol% of $TiSi_2$. From this figure, it is found that $TiSi_2$ grows only in the powder-rich area. Indeed, the calculated driving forces evidence that the one of SiC is much higher than $TiSi_2$ which is favorable only in a composition range close to the $TiSi_2$-SiC

lie-line (Figure 8-c)). One can then deduce that the reactive infiltration process should be related to the one of the eutectic liquid but with two differences (Figure 7-b)): firstly, a higher quantity of TiC may be dissolved, and, secondly, the precipitation of SiC and $TiSi_2$ may not occur in parallel, SiC being theoretically formed first. In both cases of reactive infiltration, two compacts were elaborated and infiltrated, one realized with α-SiC and the other one with β-SiC. As reported in Table 1, in each case, only one compact contains the theoretical $\frac{m_{TiC}}{m_{SiC}}$ ratio to produce a composite containing only of $TiSi_2$ and SiC. This was done to limit the local formation of deleterious pure silicon in the composite. Indeed, the melting temperature of this element is equal to 1410°C and the temperature of formation the $TiSi_2$-Si eutectic liquid is of only 1330°C, which dramatically limits the applications of such a material. The excess of TiC is expected to compensate for the eventual losses of titanium and carbon in the melt. The final composition of the samples containing TiC in excess should include a weak quantity of the ternary compound Ti_3SiC_2 without deleterious effects. The corresponding compositions called **X'** and **Y'** are indicated in orange in Figures 3-b,c).

3.2 Infiltration of SiC and TiC+SiC compacts

3.2.1 SiC compacts infiltrated by molten $TiSi_2$

The Figures 9-a,b) show the optical and the colored backscattered electrons cross-section images of the α-SiC and β-SiC compacts infiltrated by molten $TiSi_2$ at 1550°C. The α-SiC/$TiSi_2$ compact appears to be pretty good infiltrated with some remaining porosities mostly localized at the top. The infiltration of the β-SiC/$TiSi_2$ compact is lesser extended as the top of the sample is not reached by the liquid whereas the heights of the two samples are similar. In both compacts, it must be noticed the formation of a layer on the underside and on a small height of the sides with thicknesses of about 200 µm for α-SiC powder and 300 µm for β-SiC powder. This layer is formed on the faces of the α-SiC compact on a height of 4 mm, and on a height of 17 mm for the β-SiC compact. These differences seem to be caused by a more important

reactivity between β-SiC grains and the liquid leading to the rapid formation of a thick layer which limits rapidly the infiltration. Consequently, the wetting on the faces of this compact is promoted. For each compact, the atomic compositions of inner and surface areas were measured by EDS. The localization of these areas are given by red crosses in Figures 9-a,b). In both cases, the outer layer was found from EDS analyses to be mainly composed of Ti_3SiC_2 with $TiSi_2$ and SiC as minor phases. As shown in the colored cartographies in Figures 9-a,b), the infiltrated areas are composed of SiC and $TiSi_2$ as main phases, but locally it is also found Si for both samples and also Ti_3SiC_2 for the α-SiC compact. The atomic percentages obtained from energy-dispersive X-ray spectroscopy analyses (EDS) realized on inner dense areas of at least 20.10^3 μm^2 were found to be Ti:Si:C = 9:57:34 for both compacts, the accuracy of the measurement being of ±1%. The theoretical atomic ratios are expected to be Ti:Si:C = 14:57:29, so it can be deduced a lack of titanium. WDS profiles along the length of the two compacts following the red dotted lines in Figures 9-a,b) are shown in Figures 10-a,b). In these figures, the short-dotted lines indicate the starting compositions, long-dotted lines indicate the expected final compositions, red is associated to Si, blue to C and orange to Ti, the same code is used for all samples. The positions of the corresponding measured compositions are reported in the phase diagrams at 1550°C in Figures 10-c,d). Greek crosses and red Saint Andrew's crosses indicate the compositions from WDS and EDS measurements, respectively. It is confirmed from these analyses that the mole fraction of titanium is lower than expected. The compositions are found close to the theoretical ones but slightly shifted toward SiC. The presence of porosities filled by the epoxy resin induces an overestimation of the carbon content, consequently, the most porous areas are revealed by high values of carbon concentration. Remaining sparse porosities are then present with a gradient increasing from the bottom to the top of the compact. On a general manner, it is therefore deduced that an excess of silicon occurs in both compacts with a relative homogeneity along the height. From these observations, one can deduce that the Ti_3SiC_2 layer formed on the lower faces limits the infiltration of the liquid. Titanium contained in this layer comes from the liquid, which implies that the infiltrated liquid is titanium-depleted

leading to a silicon excess in the compact. Consequently, both samples are composed of the expected phases SiC and $TiSi_2$, with some volume percent of free silicon. The presence of Ti_3SiC_2 on areas of a few tens of microns in infiltrated α-SiC-containing compact is indicated by the few crosses closest to Ti_3SiC_2 in Figure 10-c). The formation of this ternary compound can be explained first by the fact that the corresponding infiltrated liquid is richer in titanium as the layer at the surface is thinner but also by the presence of larger porosities inducing locally a larger concentration of titanium favorable to the precipitation of the ternary compound.

3.2.2 TiC/SiC compacts infiltrated by the eutectic liquid

The optical cross-sections of the α-SiC+TiC and β-SiC+TiC compacts infiltrated by the $Ti_{0.16}Si_{0.84}$ liquid at 1380°C are shown in Figures 11-a,b). In both cases, the compacts are infiltrated at the bottom and on the faces with a U-shaped border of the infiltrated zone. One has also to note the formation of a layered structure along the faces of the two compacts, this is evidenced on the colored images, shown in Figures 11-a,b), taken along the faces of the compacts. The thicknesses of these structures are irregular but the mean values are close to 200 µm and 700 µm for α-SiC+TiC and β-SiC+TiC compacts, respectively. These structures are composed of two kinds of areas: i) $TiSi_2$ + free Si; and ii) SiC grains with free Si. A swelling effect is substantially visible along the infiltrated faces of the β-SiC+TiC compacts (Figure 11-b)). A less marked swelling effect also exists for the α-SiC+TiC compact but only on the lowest faces (Figure 11-a)). From EDS analyses were measured the atomic compositions of inner and surface areas for each compact. These compositions are marked by red crosses in Figures 11-a,b). The obtained ratio are Ti:Si:C = 7:59:34 and Ti:Si:C = 9:58:33 for the α-SiC and β-SiC-containing compacts, respectively. The theoretical atomic ratios are expected to be Ti:Si:C = 14:57:29, it can be deduced a titanium defect implying the presence of free silicon. Thus, the inner infiltrated areas are composed of SiC, $TiSi_2$ and free Si. The WDS profiles on the length of the two compacts are drawn in Figures 12-a,b), and the positions of the compositions are indicated in the phase diagrams at 1380°C given in Figures 12-c,d). Once again, it is found that

the mole fraction of titanium is lower than expected and the samples have a silicon excess with a relative homogeneity along the height. These findings are in good agreement with the SEM observations. From the carbon content variations of the WDS measurements, it is deduced that the compact with α-SiC powder contains a more elevated porosities quantity. Indeed, the two compacts exhibit equivalent compositions along the height and the α-SiC+TiC compact contains an elevated quantity of porosities. The β-SiC+TiC compact exhibits the expected composition but only at the infiltration front probably because of the higher starting TiC content. The filling is incomplete in both cases and the titanium content is lower than required, inducing free silicon. The outer layered structures can be justified by the elevated expansion coefficient induced by the reaction of Equation 1. This effect is all the more marked for the β-SiC+TiC compact since it is TiC-enriched.

3.2.3 SiC compacts infiltrated by molten silicon

Figures 13-a,b) show the optical cross-sections of the α-SiC+TiC and β-SiC+TiC compacts infiltrated by liquid silicon at 1450°C. At first sight, it appears clearly that the infiltration mechanisms of these compacts are different. Indeed, the α-SiC-containing compact is partially infiltrated as it exhibits a concentration gradient of the porosities which increases from the bottom to the top. A well-infiltrated area is present at the lower part describing a U-shape with a maximum thickness of about 600 µm (Figure 13-a). Some cracks are present within this area and also at its limit with the less infiltrated area. From EDS, the atomic compositions for an area at the surface and two inner areas were measured, their positions in the compact are indicated by red crosses in Figure 13-a). At the bottom of the compact, $TiSi_2$ is the main phase corresponding to 56% of the surface, SiC represents 30% of the surface and free silicon represents 14%, corresponding to the atomic ratio Ti:Si:C = 18:63:19. This may indicate that a larger quantity of the disilicide was rapidly forms in this area. At the half height of the compact, the part of this area extending over 100 µm from the face is composed of SiC (38 vol%), $TiSi_2$ (30 vol%) and free Si (32 vol%), which corresponds to the atomic ratio Ti:Si:C = 9:66:25. The

WDS profile on the length of the compact is shown in Figure 14-a) and the positions of the compositions are indicated in the phase diagram at 1450°C (Figure 14-c)). This atomic concentration profile confirms the presence of: i) a large excess of silicon; ii) a defect of titanium; and iii) porosities mainly localized in the upper portion. As shown by the colored cartographies in Figure 13-a), two cases are observed for the lower area: either there are no remaining porosities but the presence of free silicon next to SiC and $TiSi_2$ (atomic ratio Ti:Si:C = 7:59:35 from EDS); or the porosities are not completely filled and the identified phases are SiC and $TiSi_2$. The measured titanium contents are largely lower than the theoretical value. Indeed, if silicon fills the whole porosities (50% in volume), the atomic ratio Ti:Si:C should be 19:48:33 for this sample. This indicates that a large amount of titanium of TiC is dissolved in the liquid and diffuses to the surface of the compact to form $TiSi_2$, which limits the progress of molten silicon infiltration. The filling of the β-SiC+TiC compact is almost complete as only areas on the edges of the upper part are partially filled (Figure 13-b)). But this compact presents a reaction layer on its faces. From EDS, the atomic composition of this layer was found to be Ti:Si:C = 34:34:32, so this layer is composed of $TiSi_2$ and Ti_3SiC_2, as evidenced by the colored cartography in Figure 13-b). The inner areas of the compact contain SiC, $TiSi_2$ and free silicon with a fraction of silicon increasing from the faces to the center of the compact. At the center, it is found the atomic ratio Ti:Si:C = 9:62:29. In the case of a complete filling of the pores by silicon (50% in volume), the atomic ratio Ti:Si:C would be 16:51:33 for this sample. The positions of the analysed areas are marked by red crosses in Figure 13-b). Figure 14-b) shows the WDS profile along the height of this compact and the positions of the compositions are indicated in Figure 14-d). This atomic concentration profile from WDS revealed the presence of two areas along the height of the compact. This is also evidenced by the two clouds of crosses in Figure 14-d). In the lower part, it is found an elevated fraction of titanium which is larger than the theoretical value. In the upper part, the content of titanium is very low and the overall composition is very close to that of SiC. Consequently, once again, titanium was dissolved in

the liquid, diffused to the faces but in this case, it formed a Ti_3SiC_2-$TiSi_2$ layer which may prevent the filling of the remaining pores.

4 Discussion

From the experimental results reported herein, it is evidenced that the interactions between the liquid and the powders composing the compacts (SiC with or without TiC) are complex. The obtained materials differ from the expected composites that are generally not dense and contain variable quantities of free silicon. It is also found that the growth of Ti_3SiC_2 and $TiSi_2$ on the faces of the compacts is probably the origin of the above-mentioned characteristic of the experimental materials. Indeed, their presence can justify the incomplete filling as they form a practically continuous layer which limits the subsequent progression of the infiltration. The phases composing these layers contain also high fractions of titanium. It is of importance to identify the mechanisms at the origin of these changes. They involve clearly the diffusion of chemical species, especially titanium. In the case of the $SiC/TiSi_{2,Liquid}$ systems, a layer of Ti_3SiC_2 was formed on the faces of the compacts. The presence of this phase at the SiC/Liquid interface comes from a reaction between the powder and the liquid. This was predictable as no tie-line exists between SiC and molten $TiSi_2$. As reported by several authors, local equilibria are created by reactions at the interfaces [22,23]. The diffusion path implies that: i) the mass balance must be preserved; and ii) the intrinsic diffusion of species can only proceed down their activity gradient. In the present case, we found that the activity gradients of silicon and titanium can justify the experimental observations. Figure 15-a) shows the activity diagram of silicon versus the mole fraction of titanium in the Ti-Si-C system at 1550°C. The composition of the starting liquid and pure SiC are indicated by vertical dotted lines and triangles. The activity gradient must decrease monotonously from the phases of the system having the higher silicon activity to the phases having the lower activity of this element. For the $SiC/TiSi_{2,Liquid}$ systems, the activity of silicon in isolated SiC is equal to $a_{Si}^{SiC} = 3.0\times10^{-2}$ but it increases up to $a_{Si}^{Liquid,Eq} = 5.1\times10^{-1}$ when it is in equilibrium with the Ti-richest liquid, as shown in Figure 15-a). The

silicon activity in the starting liquid obtained by the melting of $TiSi_2$ is lower, $a_{Si}^{Liquid,TiSi_2}$ = 2.8×10^{-1}. Consequently, Si in SiC is dissolved into the liquid. But the mass conservation induces the formation of another phase which in the present case is Ti_3SiC_2 accordingly with the Si-activity gradient path in Figure 15-a) and experiments. Titanium is only present in the liquid before infiltration, so its activity is the highest in this phase and null in SiC, as indicated in Figure 15-b). As mentioned above, the starting liquid increases its Si-concentration inducing the growth of Ti_3SiC_2. The particularity of the experiments lies in the filling of the porosity of the materials. It can be considered that two processes occur in parallel; one corresponds to the interfacial reactions between the solid and the liquid taking place at the surface of the compacts; the other one is the capillary infiltration of the liquid in the porosities of the compacts. Consequently, the solid/liquid interactions are complex since they take place at the surface and inside the compacts. It can be proposed that when the liquid is formed, it instantaneously begins to infiltrate the porosities and in the same time, it dissolves SiC to reach the composition of the liquid (mole ratio Ti:Si:C = 26.07:73.78:0.15) in equilibrium with SiC implying the formation of Ti_3SiC_2 at the surface of SiC. The liquid of the source drop dissolves SiC particles at the surface of the compact and grains of Ti_3SiC_2 are formed and gradually grow on the wet surfaces. In parallel, the infiltrated liquid also dissolves partially the SiC grains until reaching the composition in equilibrium with Ti_3SiC_2. The silicon excess identified for the two compacts can be explained by the consumption of titanium to form the Ti_3SiC_2 gains on the faces of the compacts. The infiltration progresses until the formation of a continuous layer of Ti_3SiC_2 on the faces of the compacts. It is to note that this layer is thicker and more extended along the faces of the β-SiC compact than α-SiC compact and in a consistent way the infiltration is lower for the first than for the former. This also shows that β-SiC is more reactive than α-SiC. In the case of the TiC+SiC/$Ti_{0.16}Si_{0.84,Liquid}$ systems, it was identified that the infiltration is limited to the bottom and to the faces of the compacts (Figures 11-a,b). It was also shown that a layer containing an elevated quantity of $TiSi_2$ appeared along the faces. The presence of free Si inside the compacts with a gradient decreasing from the faces means that the quantity of titanium in

these areas is lower than expected even for the enriched sample. It can be postulated that titanium has diffused towards the faces to precipitate $TiSi_2$ creating a barrier against liquid infiltration. From Rietveld refinement of X-ray diffraction experiment on the TiC powder, it was found that the unit cell parameter of this powder is a = 4.3269(1) Å, according to the reported data by J.C. Fernandes et al. [24], the corresponding formula is $TiC_{0.76}$ with atomic composition Ti:C = 57:43. Figure 15-c) shows the activity diagram of silicon versus the mole fraction of titanium in the Ti-Si-C system at 1380°C. The activity of Ti in $TiC_{0.76}$ at 1380°C was calculated with ThermoCalc equal to 1.56×10^{-2}, this value is indicated by a diamond in Figure 15-c). In fact, the activity of Ti in the $TiC_{0.76}$+SiC mixtures is modified as these phases are not in equilibrium. So, during the heating, they react to form a mixture of $SiC+TiC_{0.92}+Ti_3SiC_2$. In this equilibrium, the activity of Ti is found to be 3.7×10^{-5}. Whereas the activity of titanium in the starting liquid is $a_{Ti}^{Liquid,Ti_{0.16}Si_{0.84}} = 1.1\times10^{-2}$. According to Figure 15-c), the activity gradient of Ti decreases from the powder mixture to the $Ti_{0.16}Si_{0.84}$ liquid. This promotes the diffusion of Ti atoms towards the compact faces to obtain a liquid in equilibrium with SiC. The monotonously decreasing path follows by the activity gradient of Ti, shown in Figure 15-c), is in agreement with the experimental observations and measurements. It implies the formation of $TiSi_2$ and the increase of the Ti fraction in the liquid. The formation of a large quantity of this phase close to the faces induced the stratified structures of the two samples. This is all the more marked for the enriched sample as it contains a higher content of TiC and consequently of Ti atoms. In the case of the $TiC+SiC/Si_{Liquid}$ systems, the results differ between the two compacts. The α-SiC-containing compact is partially infiltrated and it was formed a continuous layer at its surface composed of $TiSi_2$, pure Si and SiC. Whereas the β-SiC-containing compact is almost entirely infiltrated with a coating composed of $TiSi_2$ and Ti_3SiC_2. In both cases, the infiltrated areas contain large quantities of free silicon, close to 20% in volume (Figures 13-a,b)). The activity of Ti in $TiC_{0.76}$ at 1450°C was calculated to 1.8×10^{-2}, this value is indicated by a diamond in Figure 15-d). During the heating, $TiC_{0.76}$ and SiC should also react to form a mixture of $SiC+TiC_{0.92}+Ti_3SiC_2$ in which the activity of Ti is found to be

6.4×10^{-5} and its activity in pure molten silicon is $a_{Ti}^{Liquid,Si} = 0.0$. So, the activity gradient of titanium is very elevated and consequently, titanium atoms should diffuse strongly through the liquid phase until its activity in the liquid is equal to $a_{Ti}^{Liquid,Eq} = 5.3\times10^{-5}$. In the activity diagram in Figure 12-d), $TiSi_2$ and Ti_3SiC_2 are not formed at the equilibrium. In other words, during the infiltration, titanium and a small fraction of carbon from TiC are dissolved in the liquid, the remaining carbon reacts with the liquid to form SiC. During the cooling, $TiSi_2$, free silicon and a small amount of SiC should be obtained due to the crystallization of the liquid. For the two compacts, the measured compositions of two internal areas are close but richer in Si than the expected theoretical compositions (Figure 14-d)). This confirms that titanium is dissolved in the infiltrated liquid and diffuse to the external drop. This implies a deficit of titanium in the compacts even for the enriched one. For the α-SiC-containing compact with a TiC excess, the infiltration should not be limited by the growth of $TiSi_2$ on the faces as the formation of this phase is not favorable according to the activity gradient of titanium. But the driving force of this phase is not null as shown in Figure 8-c), so it can be formed kinetically. This agrees with the presence of a $TiSi_2$-rich layer at the surface of the compact (Figure 13-a)) which can only be formed when the outer liquid is saturated in titanium. This is even more likely that this sample is very concentrated in titanium. The quantity of $TiSi_2$ formed is so elevated close to the surface of the compact that it implies the formation of cracks along the faces. The exothermicity of SiC precipitation during the infiltration can also be involved in the formation of $TiSi_2$. Indeed, as the solubility in titanium increases with the temperature, the oversaturated liquid leads to the precipitation of $TiSi_2$ when the temperature decreases. For the β-SiC-containing compact, an analogous mechanism can be considered but the infiltration is more important. This sample contains a lower quantity of TiC, that is why the saturation of the external liquid occurs later, just like the formation of the layer on the faces. The $TiSi_2$ grains on the faces are large, which indicates that they were formed from a liquid phase. Some grains of Ti_3SiC_2 are also present in this layer. Indeed, the measured atomic composition of this layer is Ti:Si:C = 34:34:32, the corresponding point is found in the ternary equilibrium between Ti_3SiC_2, $TiSi_2$

and SiC (Figure 14-d)). The presence of the ternary phase is quite surprising in this case. It is to note that the layer of the β-SiC-containing compact is quite similar to the ones obtained with the SiC/$TiSi_{2,Liquid}$ systems. The ternary phase is obtained by reaction between a Ti-rich liquid and SiC. It was proposed above that β-SiC reacts easier with the liquid to form Ti_3SiC_2. This process is probably at the origin of the growth of Ti_3SiC_2 whose driving force is quite elevated in Ti-rich compositions and even higher than the one of $TiSi_2$ (Figure 8-c)). In this case, β-SiC reacts quickly with the overheated and oversaturated liquid to form Ti_3SiC_2. The large sizes and angular shapes of the grains of this ternary phase are consistent with this hypothesis. These particular behaviors with molten silicon can be at least partially justify by the extremely high gradient of activity of titanium which is absent in the initial liquid. The dissolution and diffusion of titanium in the liquid are therefore very important and fast, which promotes the kinetically formation of $TiSi_2$ close to the faces. The exothermicity of SiC precipitation plays probably a determining role in the precipitation of $TiSi_2$ and Ti_3SiC_2 on the faces. It is demonstrated herein that the experimental results can be largely explained from thermodynamic calculations. This work proves that thermodynamic plays a determining role during the infiltration process. In the present case, it can be deduced that the elaboration of SiC-$TiSi_2$ composites could be possible in limiting or in prohibiting the activity gradients. On this way, a first solution could be to operate at a temperature higher than the melting point of $TiSi_2$ in using a liquid in equilibrium with the powders containing Ti, Si and C elements i.e. the activity of these three elements should be equal in all phases. Then, the composite would be obtained at the cooling. A second solution could be to work at a temperature lower than the melting temperature of $TiSi_2$ in infiltrating a Ti-rich liquid that forms only SiC and a Ti-saturated liquid, the disilicide crystallizes from the new liquid during the cooling. For both proposed solutions, the difficulty lies in the necessity to adjust the composition of the powders mixture to obtain the only desired phases and to fill the porosities. These possibilities will be shortly examined experimentally. This method seems for us relevant to many other systems implying an infiltration step.

5. Conclusion

The aim of the present work was to get a better insight into the reaction processes that may develop during the infiltration of Si-Ti molten alloys or liquid silicon into TiC-SiC compacts between 1380 and 1550°C. Thermodynamic calculations performed on these systems were found as a powerful method for a better understood of the chemical driving phenomena during the infiltration process. The experimental results show that the interface stabilization implies the dissolution of the elements in the liquids and their diffusion trough their chemical activity gradients via the liquid. That is why an enrichment in silicon of the infiltrated areas is observed because of the diffusion of titanium dissolved from TiC. In the case of the compacts containing only SiC powders, a reaction occurs with formation of a Ti_3SiC_2 coating at liquid/compact interface predictable from thermodynamic calculations. The growth of this layer limits the infiltration process and implies a Ti-defect of the infiltrated liquid. It is also proposed in the case of pure molten silicon that an extremely elevated activity gradient between the solid and the liquid promotes the kinetic growth of unexpected phases. The main finding of this work is that thermodynamic approach is a powerful method to identify the main limitations of many high temperature processes implying molten metals. It is expected that this methodology will make possible the identification of the optimal solutions for the elaboration of materials by liquid infiltration

Acknowledgement

The authors wish to thank Laurine Lapuyade and Muriel Alrivie, from the Laboratory of ThermoStructural Composites (LCTS - UMR 5801 - UB-CNRS-CEA-SAFRAN); and Michel Martineau (PLACAMAT - UMS 3626) for their kind assistance.

References

[1] R. Rosenkranz, G. Frommeyer, W. Smarsly, Microstructures and properties of high melting point intermetallic Ti_5Si_3 and $TiSi_2$ compounds, Mater. Sci. Eng. A152 (1992) 288-294. https://doi.org/10.1016/0921-5093(92)90081-B

[2] D. Vojtech, B. Bartova, T. Kubatik, High temperature oxidation of titanium–silicon alloys, Mater. Sci. Eng. A361 (2003) 50-57. https://doi.org/10.1016/S0921-5093(03)00564-1

[3] W.Y. Yang, H. Iwakuro, H. Yagi, T. Kuroda, S. Nakamura, Study of oxidation of $TiSi_2$ thin film by XPS, Jpn. J. Appl. Phys. 23 (1984) 1560-1567. https://doi.org/10.1143/JJAP.23.1560

[4] D.Y. Oh, H.C. Kim, J.K. Yoon, I.J. Shon, One step synthesis of dense $MoSi_2$–SiC composite by high-frequency induction heated combustion and its mechanical properties, J. Alloys Compd. 395 (2005) 174-180. https://doi.org/10.1016/j.jallcom.2004.10.072

[5] T.S.R.Ch. Murthy, C. Subramanian, R.K. Fotedar, M.R. Gonal, P. Sengupta, S. Kumar, A.K. Suri, Preparation and property evaluation of TiB_2 + $TiSi_2$ composite, Int. J. Refract. Metals Hard Mater. 27 (2009) 629-636, https://doi.org/10.1016/j.ijrmhm.2008.10.001

[6] H. Wu, F. Chen, J. Xu, Preparation and Characterization of (Mo,W)Si_2-SiC composites by in situ microwave reaction sintering, Mater. Eng. Perform. 26 (2017) 3239-3244. https://doi.org/10.1007/s11665-017-2775-7

[7] W. Li, K. Shirvan, U_3Si_2-SiC fuel performance analysis in BISON during normal operation, Ann. Nucl. Energy 132 (2019) 34-45. https://doi.org/10.1016/j.anucene.2019.04.021

[8] Z. Tong, R. He, T. Cheng, K. Zhang, D. Dai, Y. Yang, D. Fang, High temperature oxidation behavior of ZrB_2-SiC added $MoSi_2$ ceramics, Ceram. Inter. 44 (2018) 21076-21082. https://doi.org/10.1016/j.ceramint.2018.08.144

[9] R. Radhakrishnan, C.H. Henager, Jr., J.L. Brimhall, S.B. Bhaduri, Synthesis of Ti_3SiC_2/SiC and $TiSi_2$/SiC composites using displacement reactions in the Ti-Si-C system, Scripta Mater. 34 (1996) 1809-1814. https://doi.org/10.1016/1359-6462(95)00663-X

[10] R. Voytovych, V. Bougiouri, N.R. Calderon, J. Narciso, N. Eustathopoulos, Reactive infiltration of porous graphite by NiSi alloys, Acta Mater. 56 (2008) 2237-2246, https://doi.org/10.1016/j.actamat.2008.01.011

[11] N.R. Calderon, M. Martinez-Escandell, J. Narciso, F. Rodriguez-Reinoso, The role of carbon biotemplate density in mechanical properties of biomorphic SiC, J. Eur. Ceram. Soc. 29 (2009) 465-472. https://doi.org/10.1016/j.jeurceramsoc.2008.05.049

[12] N.R. Calderon, M. Martinez-Escandell, J. Narciso, F. Rodriguez-Reinoso, Manufacture of Biomorphic SiC components with homogeneous properties from sawdust by reactive infiltration with liquid silicon, J. Am. Ceram. Soc. 93 (2010) 1003-1009. https://doi.org/10.1111/j.1551-2916.2009.03572.x

[13] H. Matsunami, T. Kimoto, Step-controlled epitaxial growth of SiC: High quality homoepitaxy, Mater. Sci. Eng. R20 (1997) 125-166. https://doi.org/10.1016/S0927-796X(97)00005-3

[14] J. Li, D. Jiang, S. Tan, Microstructure and mechanical properties of in situ produced SiC/$TiSi_2$ nanocomposites, J. Eur. Ceram. Soc. 20 (2000) 227-233. https://doi.org/10.1016/S0955-2219(99)00157-0

[15] M. Sun, Y. Bai, M. Li, S. Fan, L. Cheng, In-situ fabrication of laminated SiC/$TiSi_2$ and SiC/Ti_3SiC_2 ceramics by liquid silicon infiltration, Ceram. Inter. 44 (2018) 11410-11416. https://doi.org/10.1016/j.ceramint.2018.03.194

[16] I.J. Shon, H.K. Park, H.C. Kim, J.K. Yoon, K.T. Hong, I.Y. Ko, One-step synthesis and densification of nanostructured $TiSi_2$–SiC composite from mechanically activated (TiC + 3Si) powders by high-frequency-induced heated combustion, Scripta Mater. 56 (2007) 665-668. https://doi.org/10.1016/j.scriptamat.2006.12.042

[17] J.O. Andersson, T. Helander, L. Höglund, P.F. Shi, B. Sundman, Thermo-Calc and DICTRA, Calphad 26 (2002) 273-312. https://doi.org/10.1016/S0364-5916(02)00037-8

[18] N. Saunders, A. P. Miodownik, and Editors., Calculation of Phase Diagrams (CALPHAD): A Comprehensive Guide. Elsevier, 1998.

[19] H.L. Lukas, S.G. Fries, B. Sundman, Computational thermodynamics: The CALPHAD method. Cambridge: Cambridge University Press, 2007.

[20] Y. Du, J.C. Schuster, H.J. Seifert, F. Aldinger, Experimental investigation and thermodynamic calculation of the titanium–silicon–carbon system, J. Am. Ceram. Soc. 83 (2000) 197-203. https://doi.org/10.1111/j.1151-2916.2000.tb01170.x

[21] C.A. Schneider, W.S. Rasband, K.W. Eliceiri, NIH Image to ImageJ: 25 years of image analysis, Nature Methods 9 (2012) 671-675. https://doi.org/10.1038/nmeth.2089

[22] F.J.J. van Loo, Multiphase diffusion in binary and ternary solid-state systems, Prog. Solid St. Chem. 21 (1990) 47-99. https://doi.org/10.1016/0079-6786(90)90007-3

[23] M. Zhe, O. Dezellus, B. Gardiola, M. Braccini, J.C. Viala, Chemical changes at the interface between low carbon steel and an Al-Si alloy during solution heat treatment, J Phase Equilib. Diff. 32 (2011) 486-497. https://doi.org/10.1007/s11669-011-9949-z

[24] J.C. Fernandes, C Anjinho, P.M. Amaral, L.G. Rosa, J. Rodriguez, D. Martinez, F.A. Costa Oliveira, N. Shohoji, Characterisation of solar-synthesised TiC_x (x = 0.50, 0.625, 0.75, 0.85, 0.90 and 1.0) by X-ray diffraction, density and Vickers microhardness, Mater. Chem. Phys. 77 (2002) 711-718. https://doi.org/10.1016/S0254-0584(02)00131-1

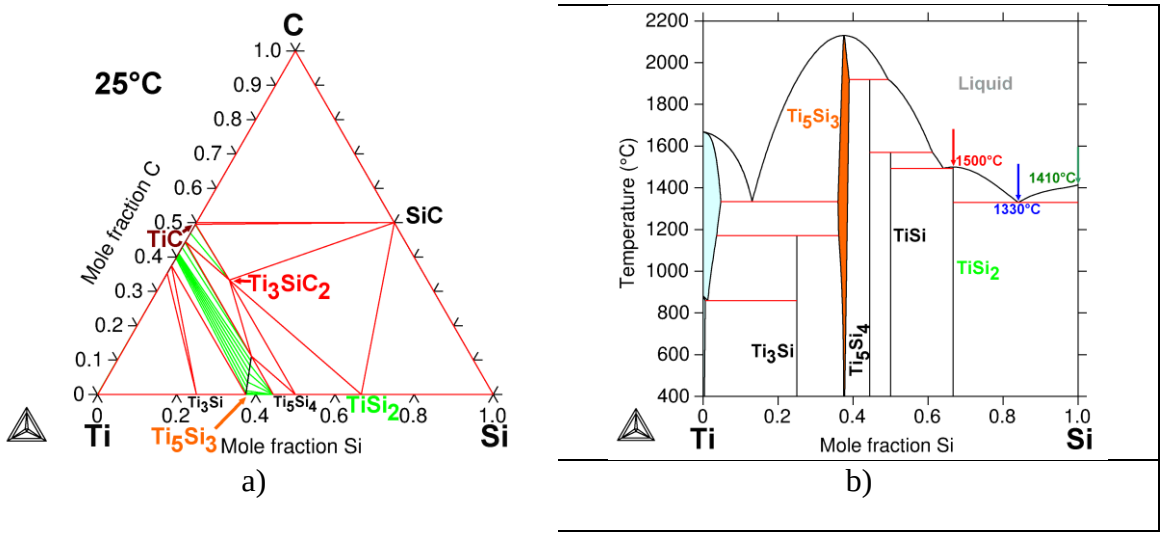

Figure 1. Ti-Si-C system: a) isothermal section at 25°C and b) Ti-Si phase diagram [20]

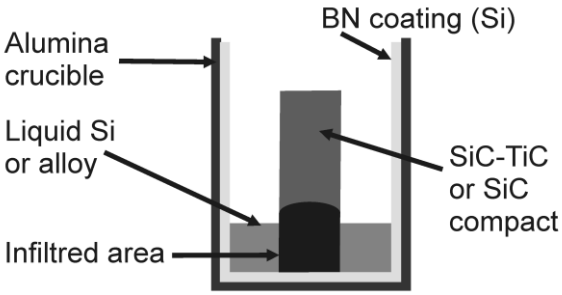

Figure 2. Experimental setup for the infiltration experiments of molten Si or Ti-Si alloys in SiC and TiC-SiC compacts

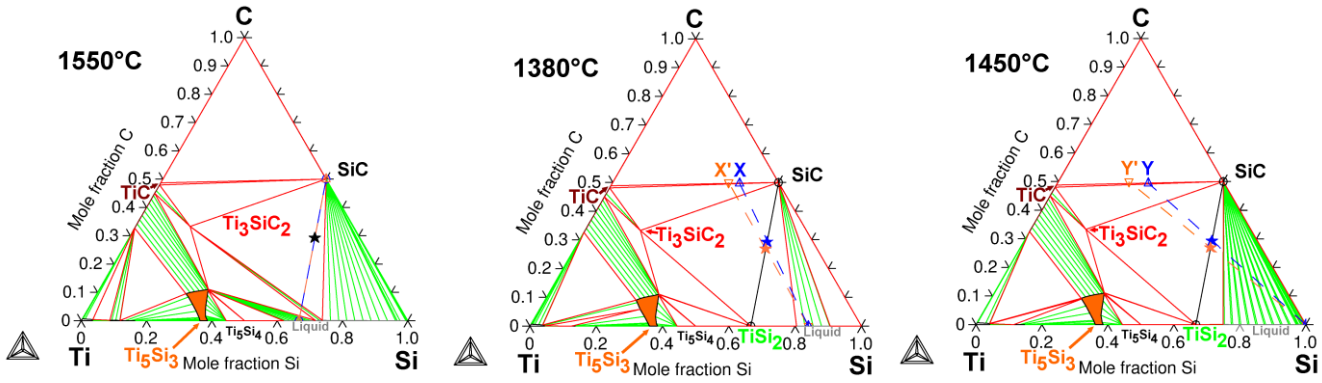

Figure 3. Isothermal sections of Ti-Si-C system at: a) 1550°C, b) 1380°C and c) 1450°C The expected compositions are indicated by 5-pointed stars.

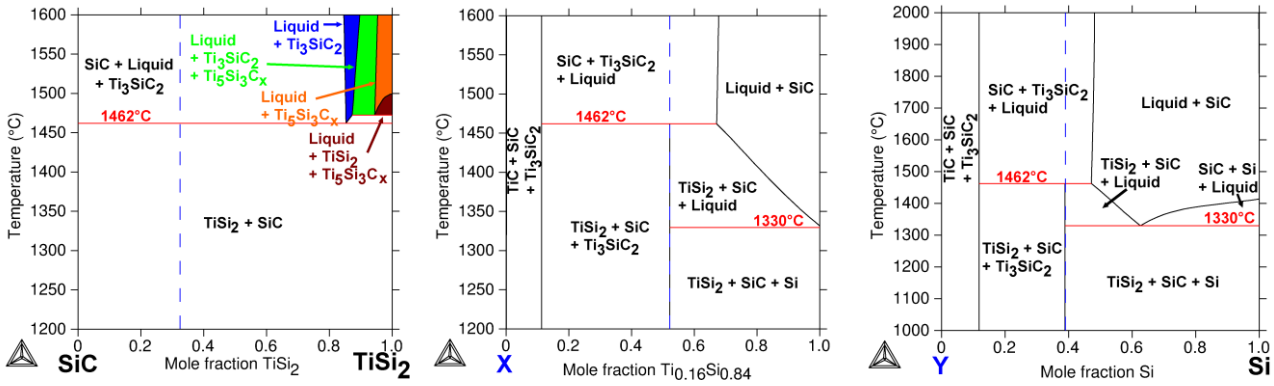

a) b) c)

Figure 4. Calculated isopleth for the line compositions: a) SiC-$TiSi_2$, b) X-$Ti_{0.16}Si_{0.84}$ and c) Y-Si (dotted blue lines indicate the position of the $TiSi_2$-SiC tie-lines)

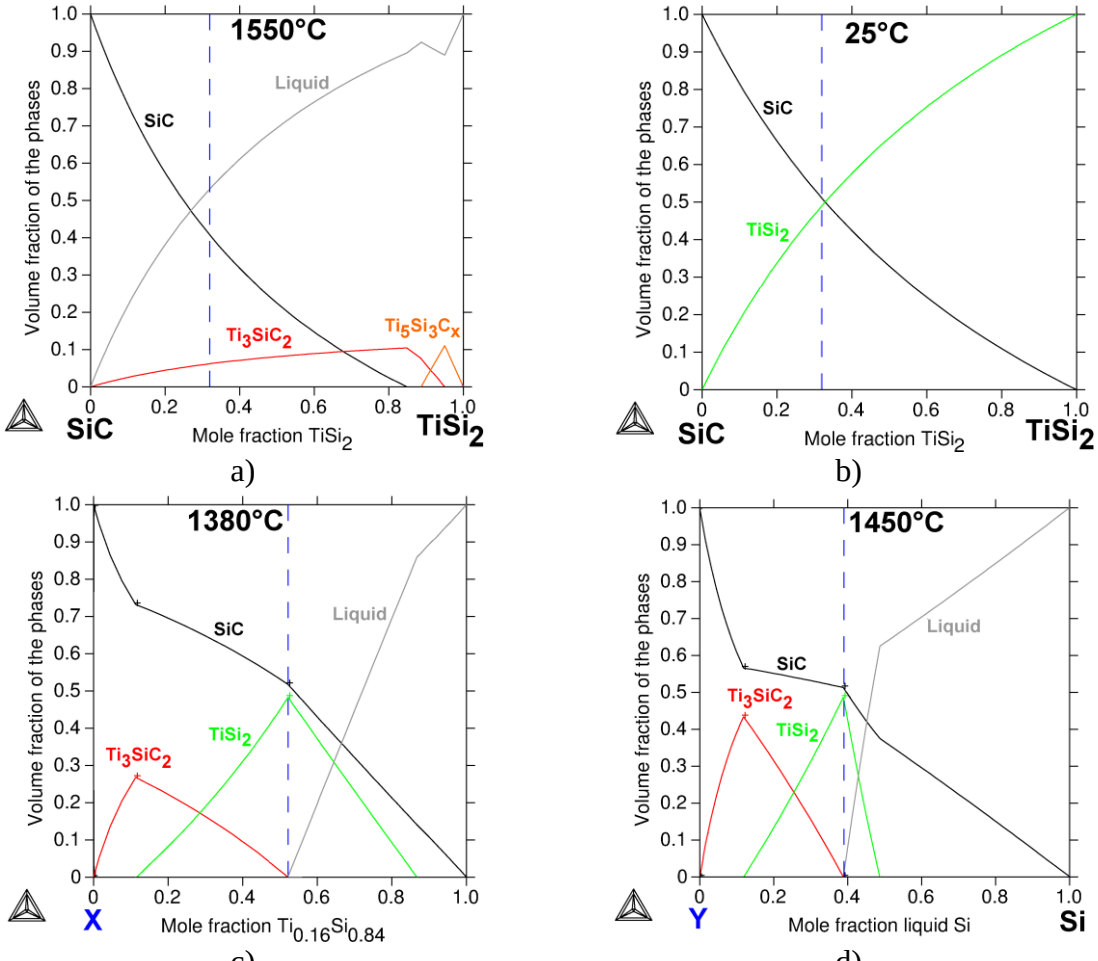

a) b) c) d)

Figure 5. Volume fraction of the phases along the line of compositions: a) SiC-$TiSi_2$ at 1550°C, b) SiC-$TiSi_2$ at 25°C, c) X-$Ti_{0.16}Si_{0.84}$ at 1450°C and d) Y-Si at 1380°C (dotted blue lines indicate the position of the $TiSi_2$-SiC tie-lines)

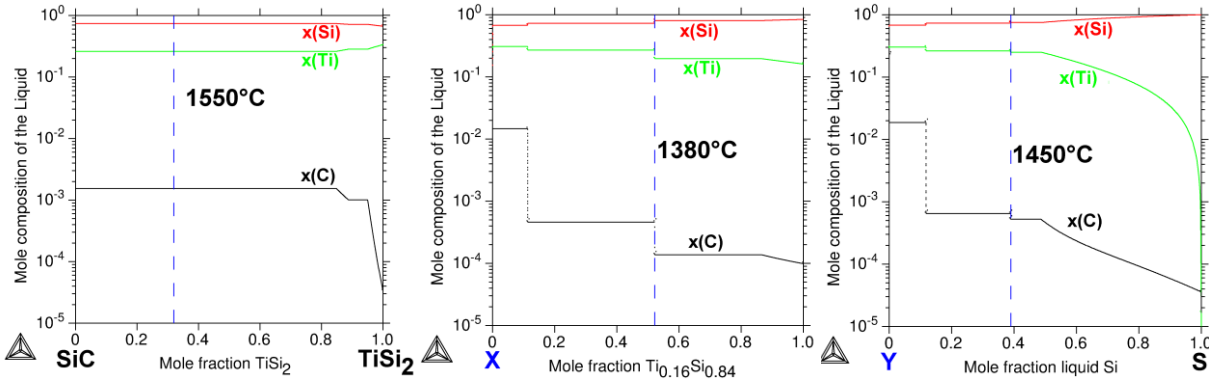

a) b) c)

Figure 6. Composition of the liquid along the line of compositions: a) SiC-$TiSi_2$ at 1550°C, b) X-$Ti_{0.16}Si_{0.84}$ at 1450°C and c) Y-Si at 1380°C (dotted blue lines indicate the position of the $TiSi_2$-SiC tie-lines)

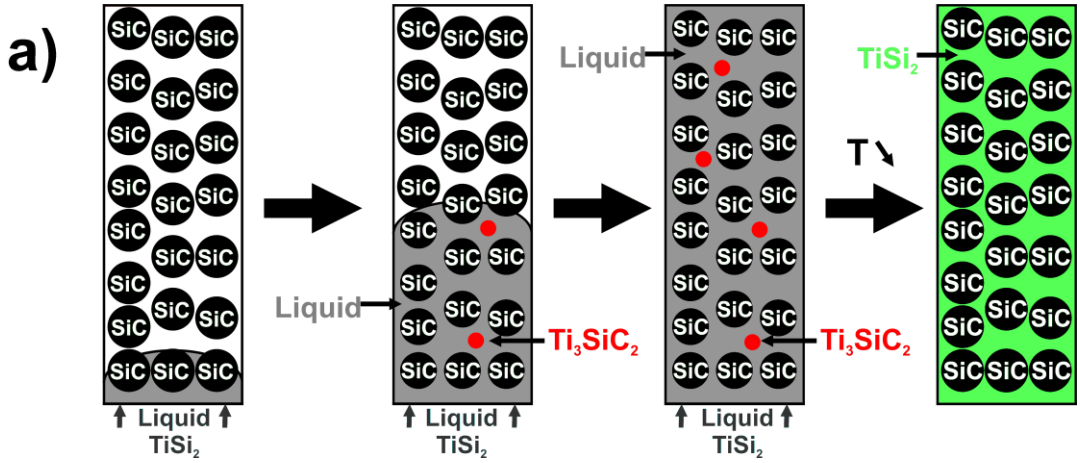

a)

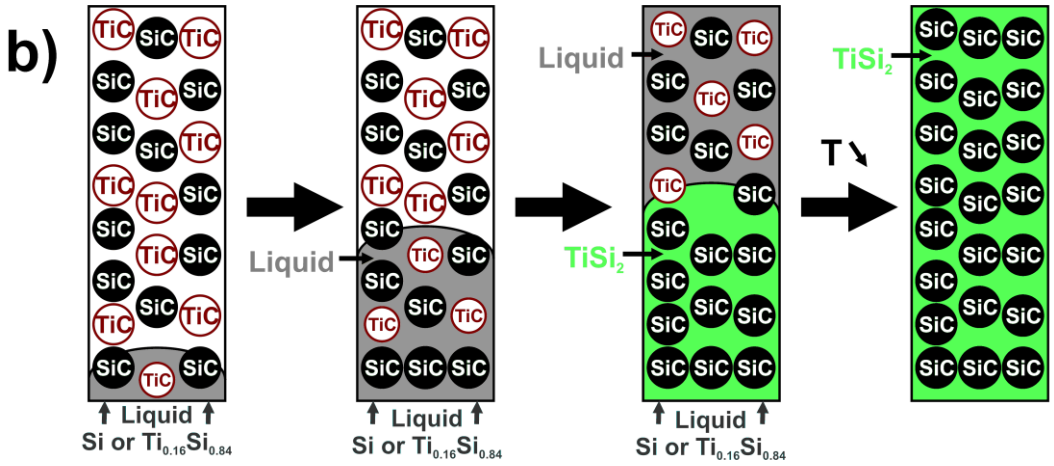

b)

Figure 7. Expected mechanisms occurring during the infiltrations of: a) liquid $TiSi_2$ at 1550°C and b) liquid Si or $Ti_{0.16}Si_{0.84}$ at 1450°C or 1380°C, respectively

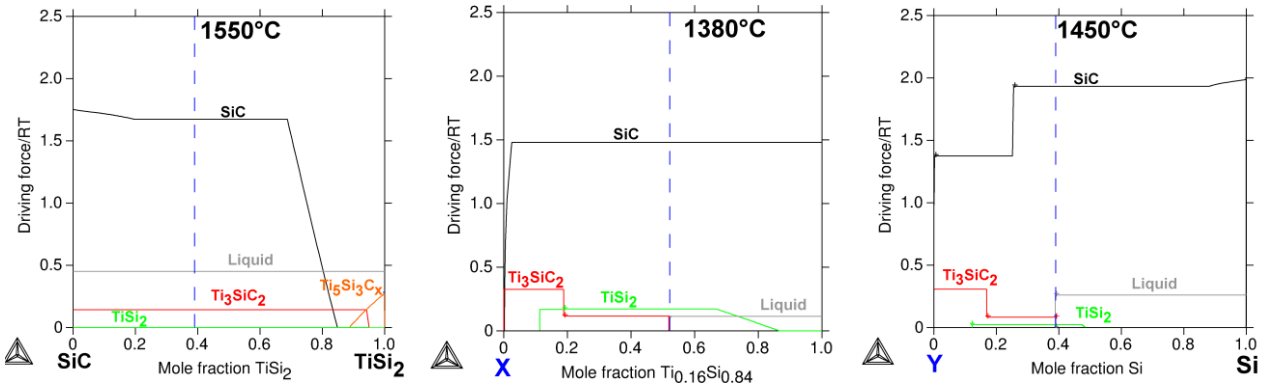

a) b) c)

Figure 8. Driving forces of the phases along the line of compositions: a) SiC-$TiSi_2$ at 1550°C, b) X-$Ti_{0.16}Si_{0.84}$ at 1380°C and c) Y-Si at 1450°C (dotted blue lines indicate the position of the $TiSi_2$-SiC tie-line)

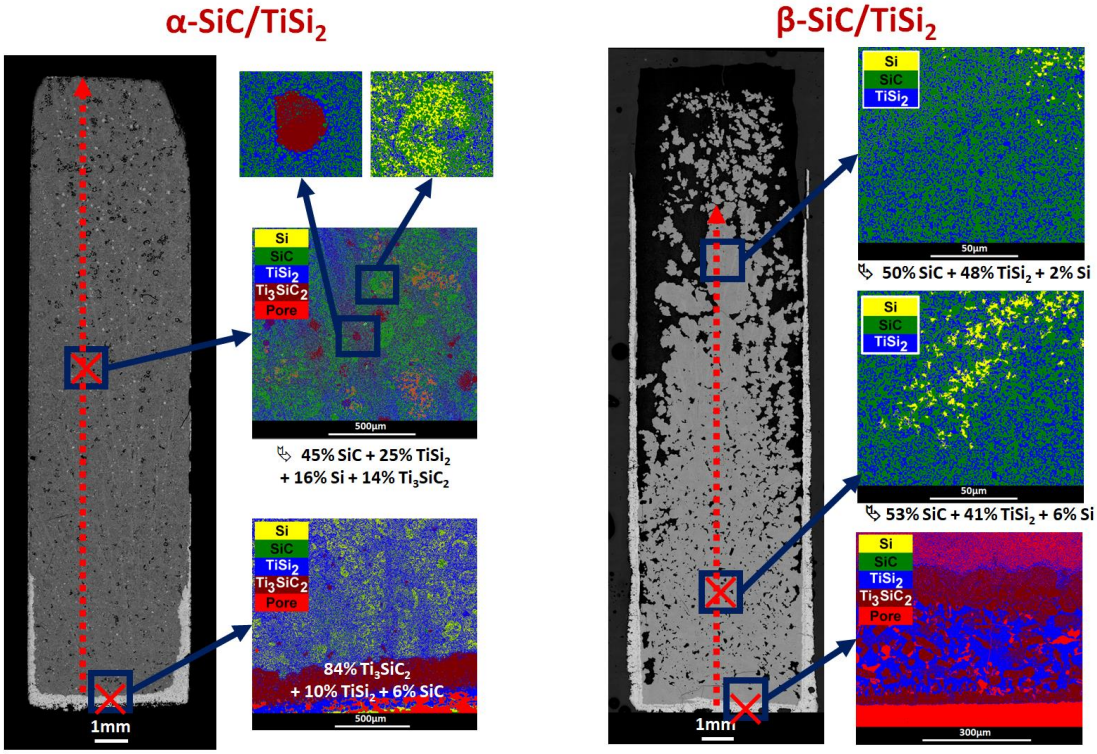

a) b)

Figure 9. Optical and colored backscattered electrons images of the cross sections of the SiC compacts infiltrated by molten $TiSi_2$ at 1550°C for 1h: a) α-SiC and β-SiC. The local surface fractions are given for whole image surface with an accuracy of ±5%.

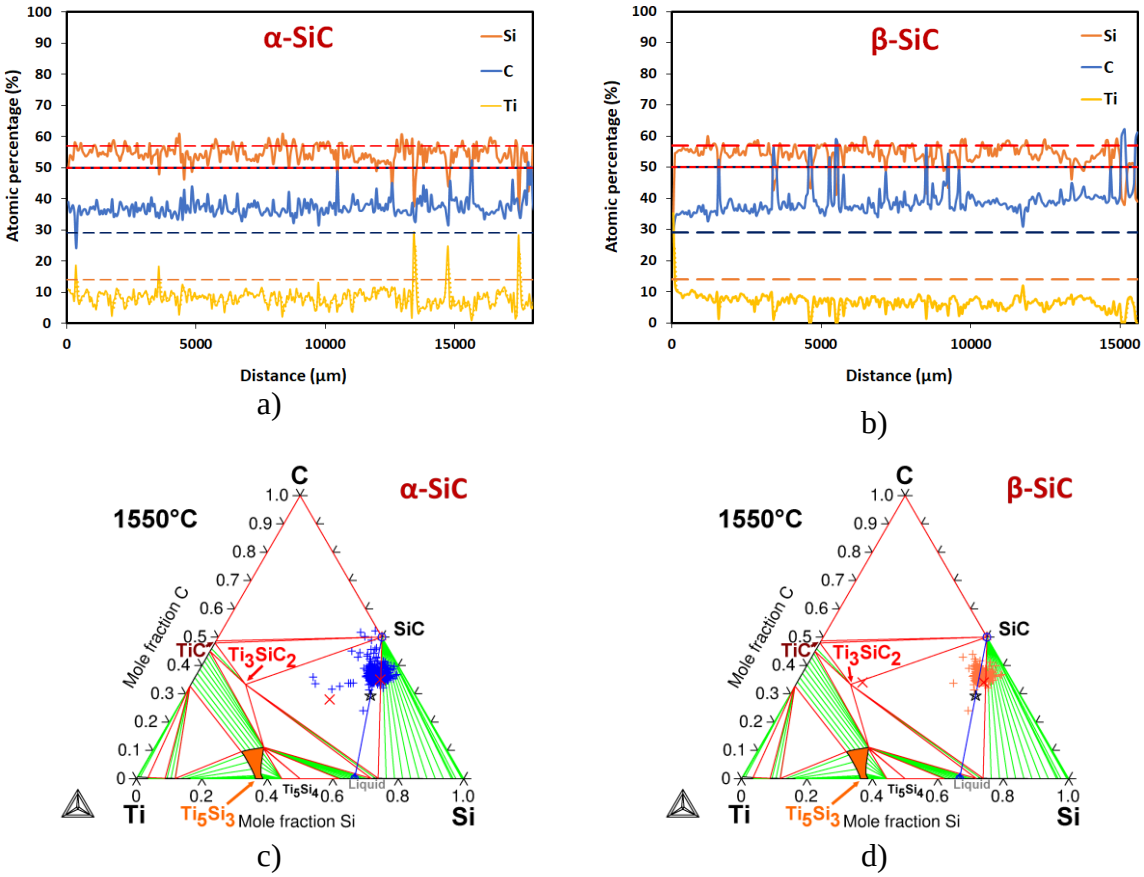

Figure 10. WDS experimental analyses on compacts infiltrated at 1550°C: (a)(b) concentration profiles of silicon, carbon and titanium corresponding to the red dotted lines in Figure 9 and (c)(d) localization of the EDS and WDS measured compositions in the corresponding Ti-Si-C phase diagram.

(the short dotted lines indicate the starting compositions, long dotted lines indicate the expected final compositions, red is associated to Si, blue to C and orange to Ti, the same code is used for all samples)

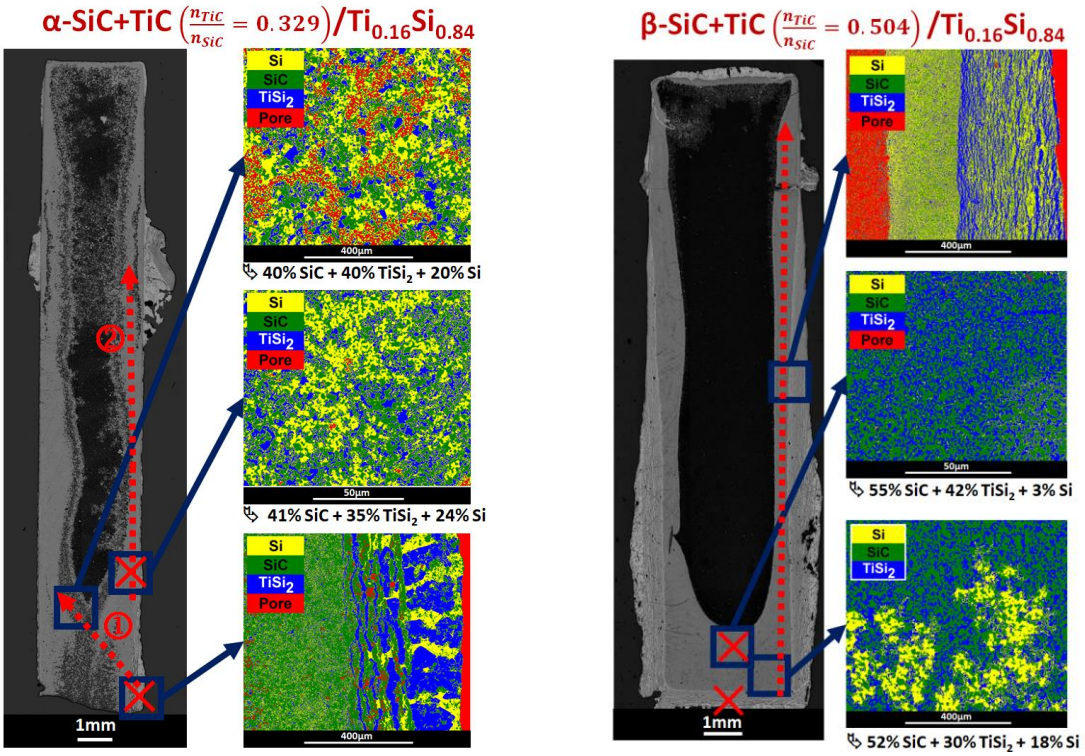

a) b)

Figure 11. Optical and colored backscattered electrons images of the cross sections of the SiC compacts infiltrated by molten $Ti_{0.16}Si_{0.84}$ at 1380°C for 1h: a) α-SiC and β-SiC. The local surface fractions are also given for whole image surface with an accuracy of ±5%.

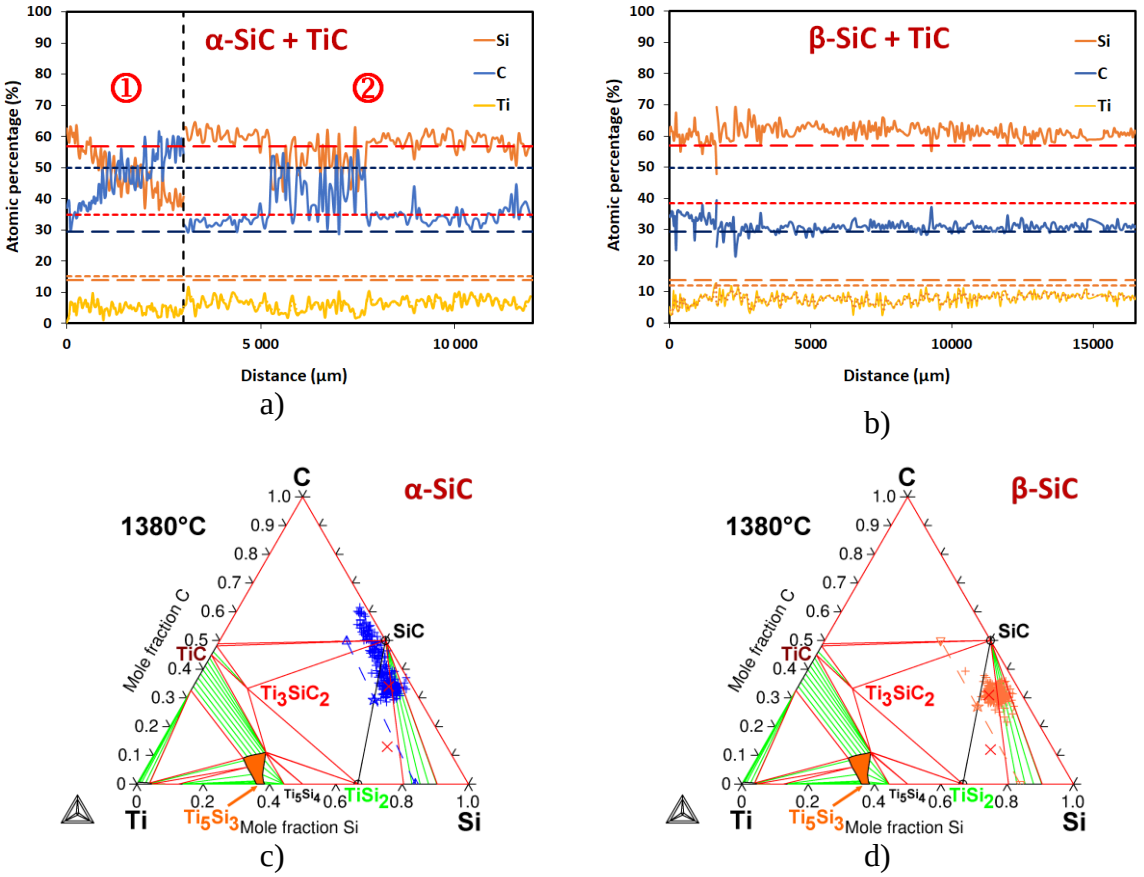

Figure 12. WDS experimental analyses on compacts infiltrated at 1380°C: (a)(b) concentration profiles of silicon, carbon and titanium corresponding to the red dotted lines in Figure 11 and (c)(d) localization of the EDS and WDS measured compositions in the corresponding Ti-Si-C phase diagram.

(short dotted lines indicate the starting compositions, long dotted lines indicate the expected final compositions, red is for Si, blue for C and orange to Ti, the same code is used for all samples)

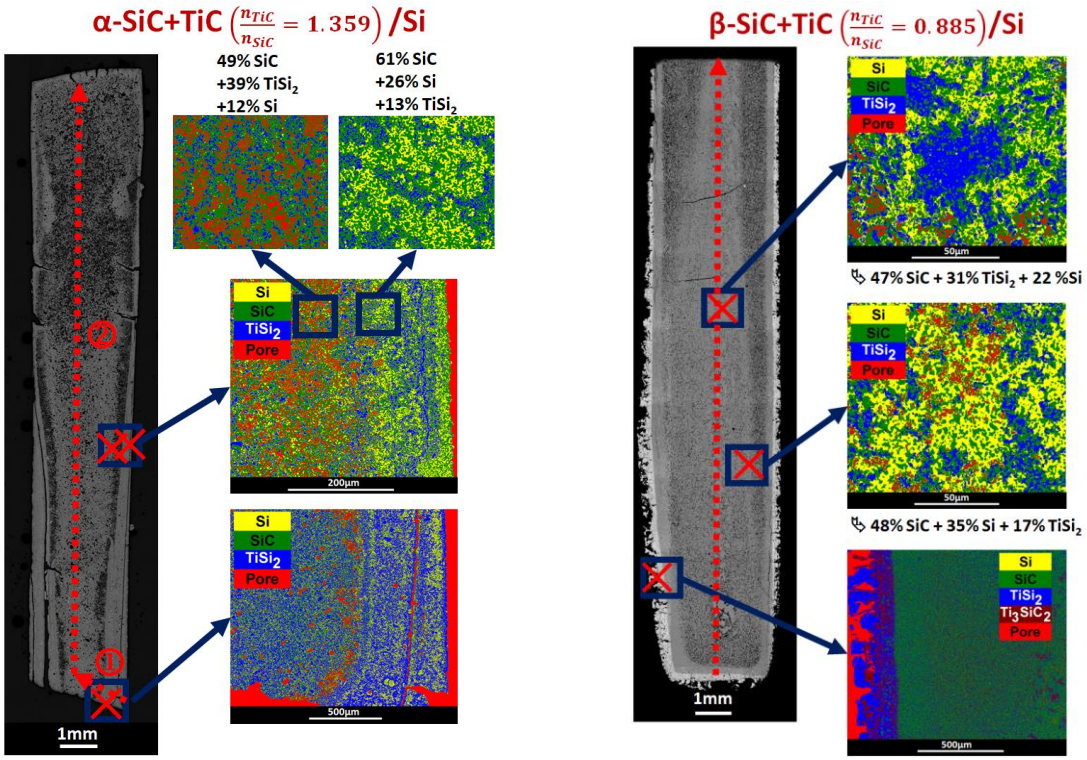

a) b)

Figure 13. Optical and colored backscattered electrons images of the cross-sections of the SiC compacts infiltrated by molten Si at 1450°C for 1h: a) α-SiC and β-SiC. The local surface fractions are given for whole images surface with an accuracy of ±5%.

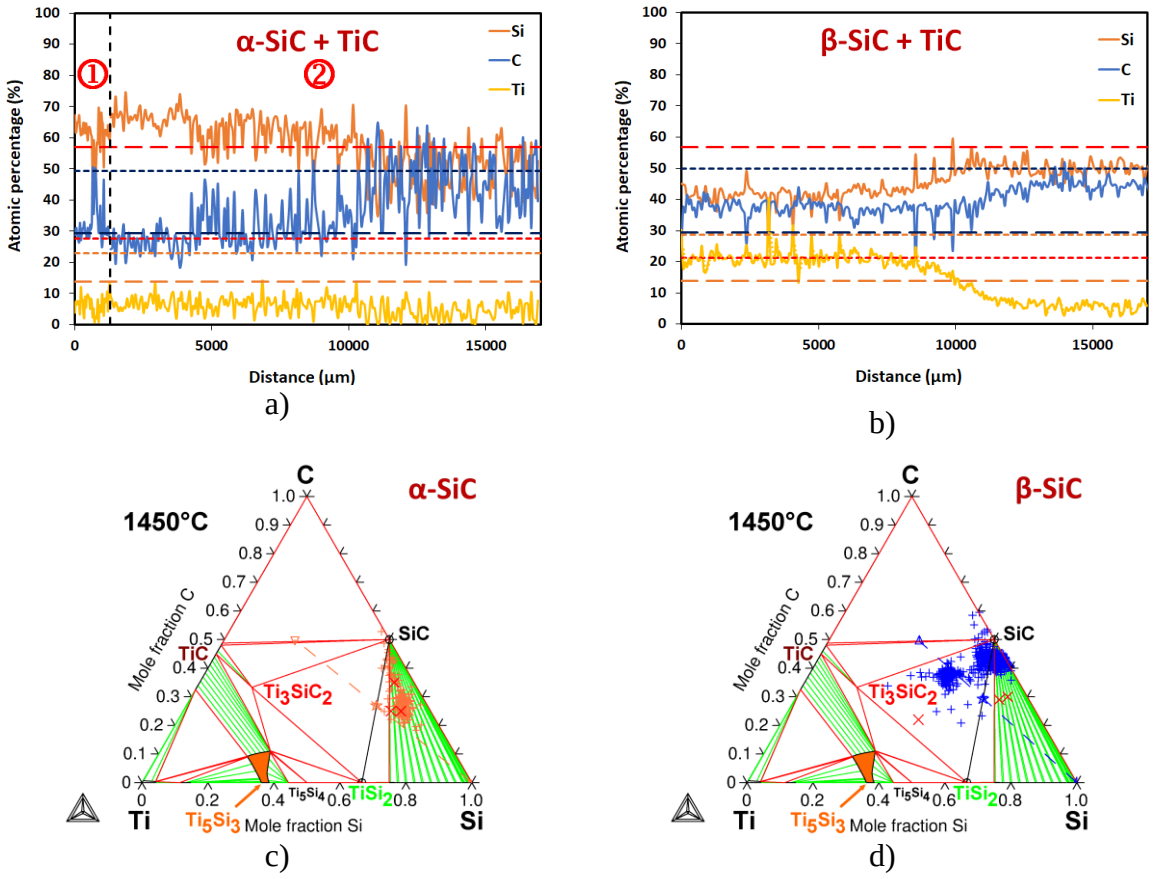

Figure 14. WDS experimental analyses on compacts infiltrated at 1450°C: (a)(b) concentration profiles of silicon, carbon and titanium corresponding to the red dotted lines in Figure 13 and (c)(d) localization of the EDS and WDS measured compositions in the corresponding Ti-Si-C phase diagram.

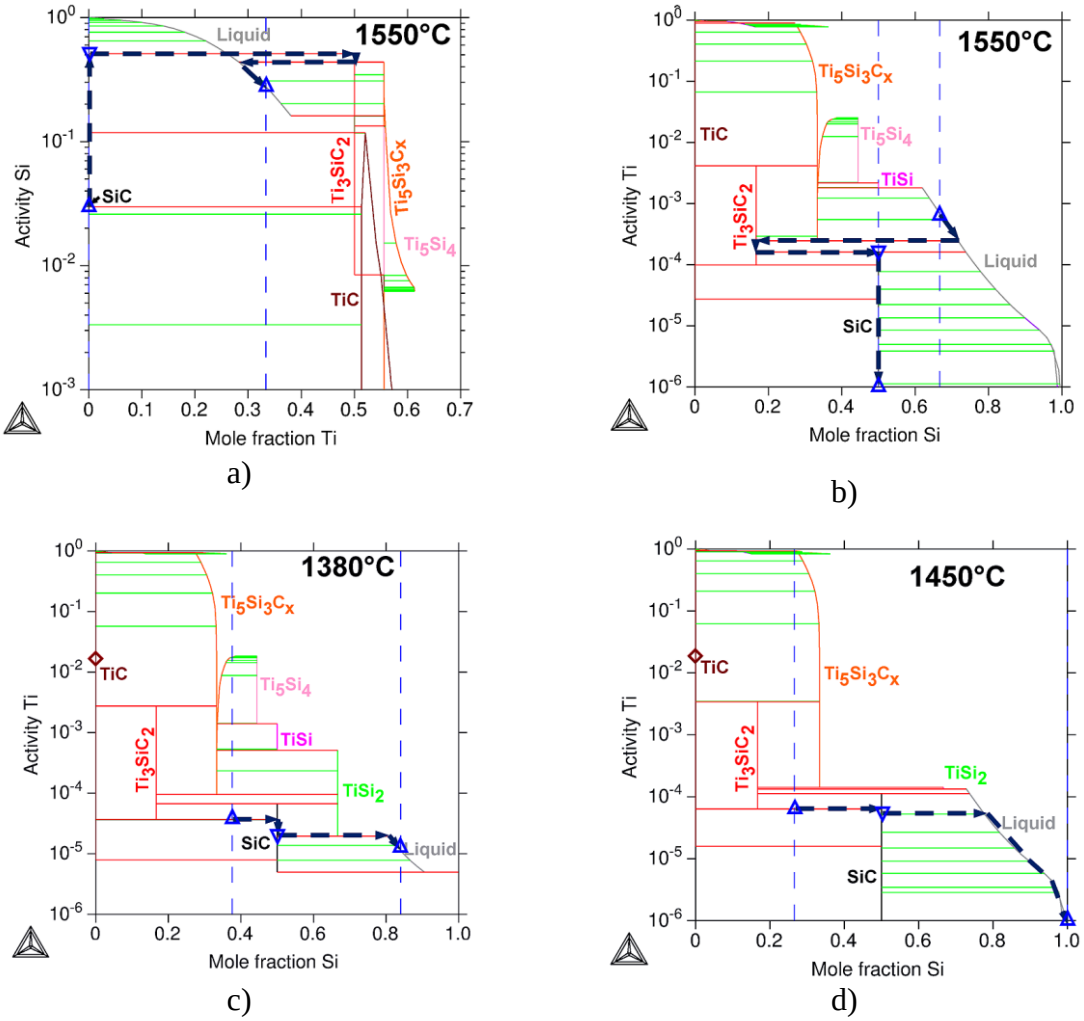

Figure 15. Calculated chemical activity along the line of compositions: a) activity of silicon in SiC-$TiSi_2$ at 1550°C, b) activity of titanium in SiC-$TiSi_2$ at 1550°C, c) activity of titanium in X-$Ti_{0.16}Si_{0.84}$ at 1380°C and c) activity of titanium in Y-Si at 1450°C (dotted blue lines indicate the compositions of the starting liquid and of the compacts, inverted triangles correspond to SiC in equilibrium with the liquid).
Liquid state was taken as reference state for silicon at 1550°C and BCC allotrope was taken as reference state for titanium

Table 1: Details about the 6 compacts used in this study

SiC polytype	Characteristics	Composition of the liquids		
		$TiSi_2$	**$Ti_{0.16}Si_{0.84}$**	**Si**
α-SiC	n_{TiC}/n_{SiC} ratio (mol)	-	0.329	**1.359**
	m_{TiC}/m_{SiC} ratio (g)	-	0.491	**2.031**
	V_{TiC}/V_{SiC} ratio (cm^3)	-	0.319	**1.320**
	Porosity (%) (±1)	49	49	49
β-SiC	n_{TiC}/n_{SiC} ratio (mol)	-	**0.504**	0.885
	m_{TiC}/m_{SiC} ratio (g)	-	**0.754**	1.322
	V_{TiC}/V_{SiC} ratio (cm^3)	-	**0.490**	0.860
	Porosity (%) (±1)	44	50	50